Highlights

Simulation of the flow past a circular cylinder from sub-critical to super-critical Reynolds numbers using an intermittency-based hybrid model

Florian Miralles, Bruno Koobus

- Investigation of a hybrid turbulence method which combines a transitional RANS model and a dynamic variational multiscale LES approach
- Application of the proposed hybrid methodology to the simulation of the flow around a circular cylinder from sub-critical to super-critical flow regimes
- Prediction of drag crisis and increase in Strouhal number using relatively coarse grids

Simulation of the flow past a circular cylinder from sub-critical to super-critical Reynolds numbers using an intermittency-based hybrid model

Florian Miralles[a,*], Bruno Koobus[b]

[a]*IMAG, Univ. Montpellier, CNRS , Montpellier, France*
[b]*IMAG, Univ. Montpellier, CNRS , Montpellier, France*

Abstract

In this work, we investigate the prediction of the flow around a circular cylinder from sub-critical to super-critical Reynolds numbers using a hybrid approach which combines a dynamic variational multiscale (DVMS) large-eddy simulation (LES) model and a transitional RANS model. In the proposed hybrid approach, the variational multiscale model, aiming to limit the effects of the subgrid-scale (SGS) model to the smallest resolved scales, is combined with the dynamic procedure which provides a tuning of the SGS dissipation in space and time. For representing laminar to turbulent boundary layer transition, the equations of the RANS part of the hybrid approach are completed with a transition model based on an intermittency transport equation. Results are compared to those of other numerical simulations in the literature and with experimental data. They highlight the overall good prediction capabilities of the proposed hybrid strategy for the simulation of such massively separated flows, even with the use of coarse meshes. In particular, the intermittency-based hybrid model was found to be able to predict the drag crisis of a circular cylinder, as well as the sharp increase in vortex shedding frequency, unlike the equivalent hybrid approach when no laminar-turbulent transition model is introduced.

Keywords: Circular cylinder, sub-critical, critical and super-critical

*Corresponding author
Email addresses: florian.miralles@umontpellier.fr, florian.miralles.itec@gmail.com (Florian Miralles), bruno.koobus@umontpellier.fr (Bruno Koobus)

Reynolds numbers, drag crisis, intermittency model, variational multiscale model, dynamic procedure, hybrid approach

1. Introduction

The flow around a circular cylinder is an important type of flow that occurs in many engineering applications and in the environment. It is an interesting and important benchmark for CFD computations, because, although the geometry is simple, the physics of this flow is complex, varies with the Reynolds number and involves a rich variety of physical phenomena. These include boundary layers, flow separations due to adverse pressure gradients (not due to geometric singularities, which increases the difficulty of prediction), shear layers, laminar to turbulent transition, and shedding of vortex structures that are convected downstream and may be eventually broken up and diffused by turbulent motion. Different flow regimes can be distinguished depending on the range of Reynolds number (Re) considered: sub-critical, critical, super-critical and trans-critical (see, for example, [1, 2, 3]).

In the sub-critical regime ($10^3 < \mathrm{Re} < 2 \times 10^5$), the boundary layers separate in the laminar regime and the transition to turbulence occurs in the separated shear-layers. The separation is early, leading to a large wake and a high value of the drag coefficient of the order of 1.2, the Strouhal number being approximately 0.2.

For $2 \times 10^5 < \mathrm{Re} < 5 \times 10^5$, the critical regime is reached. The boundary layer remains laminar on one side of the cylinder. On the other side, the boundary layer is partly turbulent (transition to turbulence occured) and detaches further downstream from the obstacle, which results in a sudden decrease in the drag coefficient down to a minimum value of around 0.2. This phenomenon is known as drag crisis. Asymmetric forces acting on the cylinder surface are then observed with a non-zero mean lift coefficient. It is also seen that the Strouhal number increases sharply and that the separation angle increases up to 130-140 degrees.

In the super-critical regime ($5 \times 10^5 < \mathrm{Re} < 2 \times 10^6$), the laminar to turbulent transition occurs in the boundary layer on each side of the cylinder, leading to a late separation and a thinner wake compared to the sub-critical case. The separation angle reduces from 140 degrees to 120 degrees, resulting in an increase of the drag coefficient with the Reynolds number.

The Reynolds number range $2 \times 10^6 < \mathrm{Re} < 4 \times 10^6$ corresponds to the trans-critical regime. The boundary layers separate in the turbulent regime

with a laminar-turbulent transition in the front part of the cylinder. The drag coefficient continues to increase and reaches a plateau up to a value of 0.5-0.6. It is also observed that the Strouhal number decreases.

The flow past a circular cylinder therefore constitutes an interesting and challenging test case for evaluating the performance of a turbulence model, especially if a wide range of Reynolds numbers is considered. RANS models, which are widely used, generally struggle to provide accurate predictions for flows with massive separation, as for instance flows around bluff bodies. An alternative approach is large-eddy simulation (LES), which is more accurate for massively separated flows but more computationally expensive than RANS. Indeed, the LES grid must be fine enough to resolve a significant part of the turbulent scales, and this becomes particularly critical in the regions close to the wall. Moreover, the cost of LES increases with the Reynolds number. In this context, hybrid strategies have been proposed in the literature, which combine the RANS and LES approaches (see [4, 5, 6, 7] for a review).

Among the publications dealing with the simulation of circular cylinder flows by hybrid methods, one can mention the work of Travin et al. [65] in which Spalart-Allmaras Detached Eddy Simulations (DES) past a circular cylinder were performed in sub-critical and super-critical regimes. In this study, the inflow eddy viscosity is set to zero in the laminar-separation cases and to a non zero value in the turbulent-separation cases in order to manage the transition. Another interesting work is that of El Akoury et al. [66] in which, among the different turbulence models used for the simulation of a circular cylinder flow at Reynolds number 140.000, a DES/OES (Organised Eddy Simulation) and a DES based on an algebraic Reynolds stress model were applied, and for which the simulation results were compared to time-resolved PIV, phase-averaged fields and time-averaged wall pressure results.

The present work is part of a research activity aimed at developing and validating turbulence modeling approaches for the simulation of fluid dynamic problems in an industrial context. In this work, a hybrid approach blending an intermittency-based RANS model and a dynamic variational multiscale (DVMS) LES model [8] is proposed and evaluated on the simulation of circular cylinder flows. In particular, the impact of transition modeling in the hybrid simulation of such bluff body flows is investigated. The hybrid strategy adopted in this paper is based on the work presented in [9] but with a RANS part, given by the $k-\varepsilon$ model of Goldberg et al. [10], equipped with an intermittency transport equation, and the variational

multiscale model used in [9] as LES part is now combined with the dynamic procedure [8]. The proposed hybrid model enjoys attractive features such as:
i) DVMS [8] as LES part, which combines the varational multiscale approach [11], allowing the eddy-viscosity introduced by the LES closure to be restricted to the smallest resolved scales, with the dynamic procedure, [12, 13] providing a tuning of the SGS disspation in space and time, allows to reduce the often excessive damping introduced by SGS eddy-viscosity models. This is an interesting and important feature when considering scale-resolving simulation of turbulent flows, in particular those characterized by strong unsteadiness and vortices that can possibly be transported over a significant distance.
ii) In the RANS part, the selected $k - \varepsilon$ model [10], which shows ability to properly predict separated flows with adverse pressure gradients, is combined with a one equation intermittency model, based on the works of Akhter et al. [14, 15, 16] and Menter et al. [17], which allows to represent laminar to turbulent transition. These phenomena, separation induced by adverse pressure gradients and transition, often occur in engineering problems, and it is therefore important that the selected turbulence approach can properly take them into account.
iii) The blending strategy, in which the closure terms provided by a RANS and a subgrid-scale (SGS) eddy-viscosity model are blended together through the introduction of a blending function [9], permits a natural integration of the DVMS approach.

The above hybrid model is herein applied to the simulation of the flow past a circular cylinder for flow regimes ranging from sub-critical to supercritical using a mixed finite element-finite volume framework. The objective is to assess the ability of the hybrid model to predict, using grids with a not too large number of nodes (about 0.6 million), massively separated flows presenting various physical features that are encountered in engineering applications and whose physics changes significantly with the Reynolds number. Particular attention is paid to the prediction of the drag crisis which is a challenging phenomenon to capture for turbulence models. Many publications deal with the simulation of the flow around a circular cylinder, but there are only few works in the literature investigating the drag crisis phenomenon using three-dimensional computational methods (some contributions can be found in [18, 19, 20, 21, 22, 23, 24, 25]), with results not always satisfactory mainly due to insufficiently accurate turbulence models. Among these publications dealing with the drag crisis, one can mention the work of Lehmkuhl

et al. [18, 19] whose numerical results obtained with LES on fine meshes can be considered as reference numerical data due to the detailed analysis performed of the simulated flows and the prediction accuracy achieved.

The remainder of this paper is organized as follows.
In the next section, we specify the ingredients of the hybrid turbulence approach used in this work. In particular, some details are given on the transitional RANS model and the DVMS approach which are combined in the proposed hybrid strategy. In Section 3, we give some information about the numerical discretization based on a mixed finite element-fine volume formulation. In Section 4, the hybrid model is applied to the simulation of the flow around a circular cylinder for flow regimes ranging from sub-critical to super-critical, with an emphasis on the drag crisis phenomenon. Based on the numerical results obtained for this flow problem, conclusions are formulated in Section 5.

2. Turbulence modeling

In this section, we specify the three key ingredients of the proposed hybrid approach, namely the RANS part, the LES part and the hybridization strategy.

2.1. Transitional RANS model

The baseline RANS model used in our hybrid approach is the $k-\varepsilon$ model proposed in Goldberg et al. [10]. This low-Reynolds RANS model was designed to improve the predictions of the standard $k-\varepsilon$ one for adverse pressure gradient flows, including separated flows, which is an interesting feature for the prediction of many academic and industrial flows such those considered in this study.

According to the Reynolds number considered, the flow past a circular cylinder can be characterized by laminar-turbulent transition in the boundary layers, and the correct capture of this mechanism is essential for an accurate prediction of these flows. The transition, a complex phenomenon encountered in many engineering applications and which concerns the whole process of passing from a laminar to a turbulent flow, is a challenging problem to take into account by any RANS model. Among the CFD transition methods proposed in the literature (see [26, 27] for a review), the intermittency approach was chosen in this work to modify the baseline RANS model with the aim of improving its capability for capturing laminar to turbulent

transitions. In a first attempt, we combined the one equation intermittency model of Akhter et al. (details can be found in [14, 15, 16]) with our baseline $k-\varepsilon$ model. This choice was motivated by the fact that, on the one hand, this model is quite simple since it is based on only one transport equation governing the intermittency factor γ which defines the fraction of time during transition for which the flow is turbulent, and on the other hand, it has shown good abilities to predict boundary layer transition under the influence of free stream turbulence and pressure gradient for a flat plate and a turbine engine. However, as will be seen later, this intermittency model combined with the $k-\varepsilon$ of Goldberg et al. failed in predicting the flow around a circular cylinder in the supercritical regime. Following the work of Menter et al. [17], the model of Akhter et al. [14, 15, 16] was modified so that the intermittency factor γ no longer acts on the eddy viscosity but on the production and destruction terms in the transport equation governing the turbulent kinetic energy k of the baseline RANS model, and a zero normal flux is also imposed on γ at the wall.

The resulting intermittency-based $k-\varepsilon$ model used in our hybrid approach to deal with the boundary layer region is then given by:

$$\frac{\partial \rho k}{\partial t} + \nabla \cdot (\rho \mathbf{u} k) = \widetilde{P_k} - \widetilde{D_k} + \nabla \cdot [(\mu + \mu_t \sigma_k) \nabla k]$$

$$\frac{\partial \rho \varepsilon}{\partial t} + \nabla \cdot (\rho \mathbf{u} \varepsilon) = (c_{\varepsilon_1} P_k - c_{\varepsilon_2} D_k + E) T_t^{-1} + \nabla \cdot [(\mu + \mu_t \sigma_\varepsilon) \nabla \varepsilon] \tag{1}$$

$$\frac{\partial \rho \gamma}{\partial t} + \nabla \cdot (\rho \mathbf{u} \gamma) = c_{g_1} \gamma (1-\gamma) \frac{P_k}{k} + \rho c_{g_2} \frac{k^2}{\varepsilon} \nabla \gamma \cdot \nabla \gamma + \nabla \cdot [\sigma_\gamma (\mu + \mu_t) \nabla \gamma]$$

$$\widetilde{P_k} = \gamma P_k \tag{2}$$

$$\widetilde{D_k} = \max(\gamma, 0.1)\, D_k \tag{3}$$

$$\mu_t = c_\mu f_\mu \frac{k^2}{\epsilon} \tag{4}$$

$$c_{g_1} = 0.19 \quad c_{g_2} = 1.0 \tag{5}$$

where P_k and D_k are the production and destruction terms from the turbulent kinetic energy equation of the $k-\varepsilon$ model of Goldberg et al. (for details

and constants see [10]). From the above equations, one can notice that the baseline RANS model is recovered for an intermittency value $\gamma = 1$ (fully turbulent mode).
Following the work of Akhter et al. [14, 15, 16], the production term of turbulent kinetic energy is set to zero before the onset of the transition location predicted by the empirical correlation of Abu-Ghannam et al. [28]:

$$Re_{\theta,S} = 163 + \exp(6.91 - Tu) \tag{6}$$

where $Re_{\theta,S}$ denotes the Reynolds number based on the momentum thickness at the transition onset location and Tu is the turbulence intensity. Although the empirical correlation (6) is rather simple, this approximation was found to be appropriate in the simulations performed by Akhter et al. [14, 15, 16] for the prediction of transitional flows in turbine blade and flat plate.

With the objective of carrying out hybrid simulations of circular cylinder flows involving possibly transitional boundary layers, the proposed intermittency-based $k - \varepsilon$ model was evaluated on the flow around a circular cylinder at Reynolds number 10^6 (based on the far-field velocity and the cylinder diameter). For this simulation, the computational domain is a cylinder of diameter 20 times larger than the obstacle, and with a span of 2 times the obstacle diameter. Free-slip is imposed on the side surfaces, and the flow is assumed to be periodic in the spanwise direction. The inflow Mach number is set to 0.1 so that the compressibility effects can be considered as negligible, and the inflow turbulence intensity is set to 0.6 %. The mesh of 6×10^5 vertices is radial with a first layer of vertices corresponding to a dimensionless wall distance of $y^+ = 1$ and with an expansion ratio in the near wall region of 1.08. On the other hand, a uniform meshing along the azimuthal and spanwise directions is used with 400 and 30 points, respectively, on the cylinder surface along these directions.

The main bulk flow parameters predicted by the proposed transition model are summarized in Table 1, together with some experimental data. The results obtained with the intermittency model of Akhter et al. are also reported. One can notice the important improvement brought by the present transition model for all the bulk coefficients presented in this table. The RANS approach based on the transition model of Akhter et al. was unable to properly account for the transitional boundary layer leading to an early flow separation and a too high drag coefficient. The distribution over the cylinder surface of the mean pressure coefficient, shown in Fig. 1, confirms this trend.

As will be seen in the applications part, the good behavior of this transitional RANS model will be confirmed by hybrid calculations of the flow past a circular cylinder at different flow regimes.

	$\overline{C}_d$	C'_l	$-\overline{C}_{pb}$	θ_{sep}
Present simulation				
URANS $k-\varepsilon-\gamma$ (model of Akhter)	0.512	0.23	0.50	110
URANS $k-\varepsilon-\gamma$ (present model)	0.261	0.02	0.25	130
Experiments				
Shih et al. [29]	0.24	-	0.33	-
Schewe [30]	0.22	0.02	-	-
Gölling [31]	0.22			130
Zdravkovich [2]	0.2-0.4	0.1-0.15	0.2-0.34	-
Roshko [1]	0.29	-	0.34	-

Table 1: Bulk coefficients of the flow around a circular cylinder at Reynolds number 10^6; $\overline{C}_d$ holds for the mean drag coefficient, C'_l is the root mean square of lift time fluctuation, $\overline{C}_{p_b}$ is the mean pressure coefficient at cylinder basis, θ_{sep} is the mean separation angle.

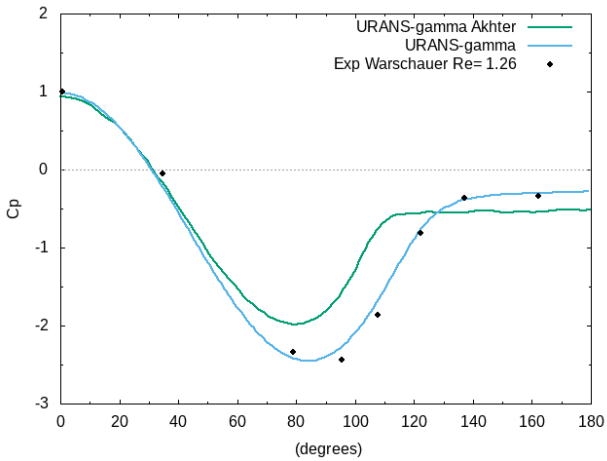

Figure 1: Flow past a cylinder at Reynolds number 10^6: distribution over the cylinder surface of the mean pressure coefficient obtained in the simulations compared to experimental data (Warschauer [57]). "URANS-gamma Akhter" holds for the baseline URANS model equipped with the intermittency model of Akhter, and "URANS-gamma" is the present intermittency-based URANS model.

2.2. LES-like model: DVMS

We now briefly present the DVMS model which is preferred to the classical LES approach in our hybrid strategy because of some specific properties, as will be specified hereafter, that allow this model to have a better behavior in some regions of the flow, such as shear layers and wakes. Further information on the description of this approach can be found in [11, 8].

The Variational Multiscale (VMS) model for the large eddy simulation of turbulent flows has been introduced in [32] in combination with spectral methods. In [11], an extension to unstructured finite volumes is defined. In the present work, this method is integrated in the hybridization strategy for the closure of the LES part. Let us explain this VMS approach in a *simplified context*. Suppose the mesh is made of two embedded meshes. On the fine mesh we have a P^1-continuous finite-element approximation space V_h with the usual basis functions Φ_i vanishing on all vertices but vertex i. Let V_{2h} represents its embedded coarse subspace. Let V_h' be the complementary space: $V_h = V_{2h} \oplus V_h'$. The space of *small scales* V_h' is spanned by only the fine basis functions Φ_i' related to vertices which are not vertices of V_{2h}. Let us denote the compressible Navier-Stokes equations by: $\dfrac{\partial W}{\partial t} + \nabla \cdot F(W) = 0$ where $W = (\rho, \rho u, E)$ are the flow variables, ρ being the density, u the velocity vector and E the total energy per unit volume.
The VMS discretization writes for $W_h = \sum W_i \Phi_i$:

$$\left(\frac{\partial W_h}{\partial t}, \Phi_i\right) + (\nabla \cdot F(W_h), \Phi_i) = -\left(\tau^{LES}({W_h}'), {\Phi_i}'\right) \tag{7}$$

where F denotes the convective and diffusive fluxes, and ${W_h}'$ represents the small scale component of the resolved flow variables W_h. For a test function related to a vertex of V_{2h}, the RHS vanishes, which limits the action of the LES term to small scales. In practice, embedding two unstructured meshes V_h and V_{2h} is a constraint that we want to avoid. The coarse level is then built from the agglomeration of vertices/cells as sketched in Fig. 2. It remains to define the modeling term $\tau^{LES}(W_h')$. This term represents the subgrid-scale (SGS) stress term, acting only on the small revolved scale component W_h', and computed from the small resolved scale component of the flow field by applying either a Smagorinsky [33] or a WALE [34] SGS model, the constants of these models being evaluated by the Germano-Lilly dynamic procedure [12, 13]. The resulting model, for which a detailed description can be found in [8, 11], is denoted DVMS in this paper. It has been checked that combining

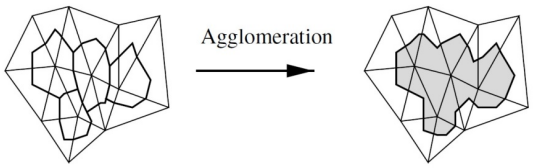

Figure 2: Building the VMS coarse level: agglomeration of some cells of the dual mesh into a macro-cell (two-dimensional case).

the VMS approach and the dynamic procedure effectively brings improved predictions [8].

A key property of the VMS formulation is that the modeling of the dissipative effects of the unresolved structures is only applied on the small resolved scales, as sketched in Fig. 3. This property is not satisfied by LES models which also damp the large resolved scales. Important consequences are that a VMS model introduces less dissipation than its LES counterpart (based on the same SGS model) and that the backscatter transfer of energy from smallest scales to large scales is not damped by the model. The VMS approach then generally allows better behavior near walls, in shear layers and in the presence of large coherent structures. Moreover, in this work, the dynamic procedure, which provides a tuning of the SGS dissipation in space and time, is combined with the VMS approach, which limits its effects to the smallest resolved scales, so that the resulting DVMS model ensures synergistic effects.

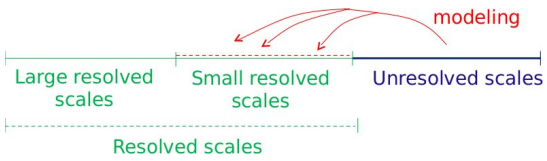

Figure 3: Modeling of the dissipative effects of the unresolved scales: VMS principle.

2.3. Hybrid strategy

The hybrid model adopted in this work is based on the work of Moussaed et al. [9]. The central idea of this approach is to combine the mean flow field obtained by the RANS part with the application of the DVMS model wherever the grid resolution is adequate. In the present hybrid approach,

the $k-\varepsilon$ model of Goldberg equipped or not with an intermittency equation (see subsection 2.1) is used as the RANS part.

Let us write, in a concise way, the semi-discretization of the RANS equations as follows:

$$\left(\frac{\partial \langle W_h \rangle}{\partial t}, \Phi_i\right) + (\nabla \cdot F(\langle W_h \rangle), \Phi_i) = -\left(\tau^{\mathrm{RANS}}(\langle W_h \rangle), \Phi_i\right) \tag{8}$$

where F represents the convective and diffusive fluxes, $\langle W_h \rangle$ denotes the RANS flow variables, $\tau^{\mathrm{RANS}}(\langle W_h \rangle)$ is the RANS closure term, and Φ_i are the basis/test functions.

Given Eqs. (7) and (8), which govern the DVMS and RANS flow variables respectively, and by introducing a blending function θ which varies between 0 and 1, a natural hybridation writes:

$$\begin{aligned}\left(\frac{\partial W_h}{\partial t}, \Phi_i\right) + (\nabla \cdot F(W_h), \Phi_i) = \\ -\theta\left(\tau^{\mathrm{RANS}}(W_h), \Phi_i\right) - (1-\theta)\left(\tau^{\mathrm{LES}}(W_h'), \Phi_i'\right)\end{aligned} \tag{9}$$

where W_h denotes now the discrete flow variables of the hybrid model. More details about the derivation of Eq. (9), not given here for brevity, can be found in [9].
From Eq. (9), we can see that the RANS approach is recovered when $\theta = 1$. Conversely, wherever $\theta < 1$, additional resolved fluctuations are computed through the last RHS term of Eq. (9), and the full DVMS approach is recovered as $\theta \to 0$.
In the numerical applications presented in this study, for which only the circular cylinder benchmark is considered, θ is set to 1 in a thin circular crown around the cylinder containing the boundary layer (i.e. the RANS model is activated), and in the remainder of the flow, θ is set to 0 (i.e. DVMS is used), with a smooth transition between these two regions. This zonal approach was used in the present work in order to ensure that the entire boundary layer is processed by the RANS model for all flow regimes considered in the simulations.

3. Numerical discretization

In this section, we briefly recall the main features of the numerical scheme. More details can be found in [35]. The governing equations, here the Navier-Stokes equations for compressible flows equipped with a turbulence model,

are discretized in space using a mixed finite element-finite volume method which applies to tetrahedrizations (unstructured or structured, depending on the geometries considered). The adopted scheme is vertex centered (i.e. all degrees of freedom are located at the vertices). P1 Galerkin finite elements are used to discretize the diffusive terms. A dual finite-volume grid is obtained by building a cell Ci around each vertex i. The convective fluxes are discretized on this tessellation by a finite-volume approach using the approximate Riemann solver of Roe [36] with low-Mach preconditioning [37]. The MUSCL linear reconstruction method (Monotone Upwind Schemes for Conservation Laws), introduced by Van Leer [38], is adapted for increasing the spatial accuracy. The basic idea is to express the Roe flux as a function of reconstructed values of W at the boundary between two neighboring cells. Attention has been dedicated to the dissipative properties of the resulting scheme, which is a key point for its successful application to LES and hybrid simulations. The numerical dissipation in the resulting scheme is made of sixth-order space derivatives using suited reconstructions [35]. Moreover, a tunable parameter directly controls the amount of introduced numerical viscosity, which allows to reduce it to the minimal amount needed to stabilize the simulation. Time advancing is carried out through an implicit linearized method, based on a second-order accurate backward difference scheme and on a first-order approximation of the Jacobian matrix [39]. The resulting numerical discretization is second-order accurate both in time and space, with a tunable numerical dissipation proportional to high-order space derivatives.

4. Applications

In all the numerical simulations presented in this section, the computational domain is a cylinder of diameter 20 times larger than the obstacle, and with a span of 2 times the obstacle diameter, which is greater than or equal to the spanwise length used for example in the LES computations of [18, 19, 44, 54, 65]. Free-slip conditions are imposed on the side surfaces and the flow is assumed to be periodic in the spanwise direction. The inflow Mach number is set to 0.1 so that the compressibility effects can be considered as negligible, and the inflow turbulence intensity is set to 0.6 %.

Relatively coarse meshes were designed in this study, which provide sufficient resolution for a hybrid model while not being too computationally expensive. This was based on previous works by the present authors group on cylinder flow calculations and on hybrid simulations (see for example ref-

erences [8, 9]). For each investigated Reynolds number, the mesh of 609.000 vertices is radial with a first layer of vertices corresponding to a dimensionless wall distance of at most $y^+ = 1$, the expansion ratio in the near wall region being 1.08, and with a uniform meshing along the azimuthal and spanwise directions, made of 400 and 30 points respectively on the cylinder surface along these directions. The resulting meshes are regular and more refined near the cylinder, so that the boundary layer mesh resolution is sufficient for a low-Reynolds RANS model (activated via a hybrid model in our case). By way of example, the computational grid used for the simulations performed at Reynolds number 10^6 is depicted in Fig. 4 with a spanwise-cross section view around the cylinder and in the vicinity of its surface.

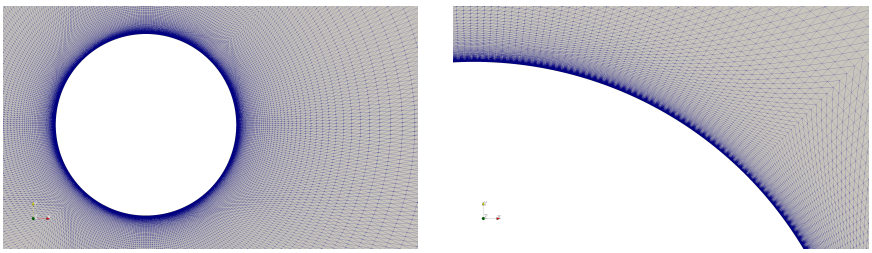

Figure 4: Computational grid: vertical cut-plane of the mesh around the cylinder and zoom close to its surface.

The time step is set to 10^-5 s, so that the sampling in time steps of the vortex shedding period is between 800 and 2100 depending on the Reynolds number. These values, which allow a fine time resolution of the flows considered in this work, correspond to a sampling in time as fine or finer than those used by our team in previous studies (see for example [8]).

For all simulations, statistics are computed by averaging in the spanwise homogeneous direction and over time for at least 25 vortex-shedding cycles (for a sensitivity of averaged quantities to the time average interval, see [40]).

Let us add that in the numerical results of the literature presented thereafter, LES simulations, most often carried out on fine grids, are preferred for comparison purposes.

4.1. Sub-critical regime

We carried out simulations at three sub-critical Reynolds numbers, namely 3900, 20,000 and 10^5. In this flow regime, the separation is laminar and occurs early, with a large wake and a high value of the drag coefficient.

The main bulk coefficients and quantities of interest are summarized in Table 2 for the different Reynolds numbers considered. They are compared with some LES results in the literature and some experimental measurements.

For Reynolds numbers 3900 and 20,000, the results obtained by the present intermittency-based hybrid model are in good agreement with the experimental data, with overall prediction accuracy as good or better than the LES simulations presented in Table 2 which are performed on finer grids (between 1.3×10^6 and 7.6×10^6 grid points for references [45, 46, 48]).

For Reynolds number 10^5, the drag coefficient is slightly overestimated with a too low value of the base pressure, while the lift fluctutations are too large. This somewhat high drag value is however more in line with the MARIN experiments obtained at a Reynolds number slightly higher than 10^5 which are given in Vaz et al. [61] and shown in Fig. 8. Very few three-dimensional simulations have been performed at this high sub-critical Reynolds number. We can mention the LES simulation of Botterill et al. [22] on a mesh of 2.5×10^6 cells. As it can be seen from Table 2, the results obtained are not in good accordance with the experimental data, which confirms the difficulty of simulating the flow past a circular cylinder at this Reynolds number.

For all the investigated Reynolds numbers, the Strouhal number, computed from spectral analysis of the lift coefficient, is well predicted showing a good agreement with the measurements. With values close to those observed in the LES simulations presented in Table 2, early separation angles are obtained by the hybrid approach based on the RANS transition model which manages to process the boundary layer in laminar mode. On the other hand, a symmetric flow separation is predicted, as shown in Fig. 10, which is confirmed by a very small mean lift coefficient (zero when rounded to two decimal places, see Table 2), as for example observed in the LES simulations of Behara et al. [44] and Yeon et al. [25] for different sub-critical Reynolds numbers.

From Table 2, we can also notice that the results are degraded with the hybrid approach using the baseline RANS model which fails to process the boundary layer in laminar mode, except for Reynolds number 3900 for which good predictions are obtained by this model. Indeed, although the hybrid approach operates in RANS mode in the near-wall region, which means here that the laminar boundary layer is handled by the baseline RANS model designed for fully turbulent flows, some RANS models, such as the one used in this study, can be able in some cases to deal with laminar boundary layers

due to the low eddy viscosity they introduce into these flow regions. This observation was also made by D'Alessandro et al. [41] who note about the behavior of different RANS models in the laminar boundary layer that *eddy viscosity is not exactly zero in the attached boundary layer, but it is small enough for its effects to be negligible*, for the Detached Eddy Simulations of the flow past a circular cylinder they performed at the same Reynolds number 3900.

The good behavior of the transitional hybrid approach, and the improvement brought by this model compared to its non-transitional counterpart, is confirmed in Fig. 5, showing the distribution of the mean pressure coefficient over the cylinder surface at Reynolds number 20,000 for which experimental data are available.

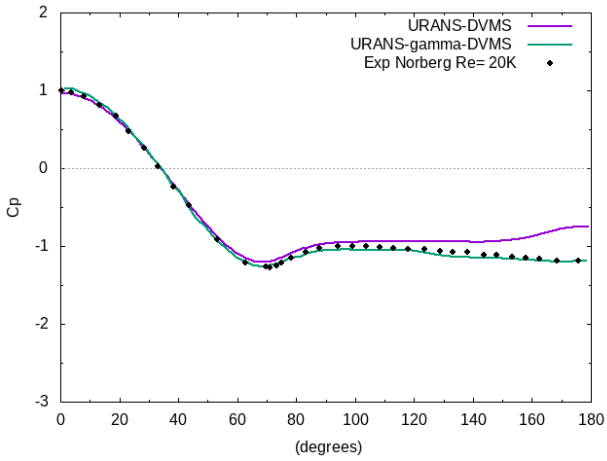

Figure 5: Flow past a cylinder at Reynolds number 20,000 (sub-critical regime): distribution over the cylinder surface of the mean pressure coefficient obtained with the hybrid model with and without transition modeling (in green and purple, respectively), compared to experimental data (Norberg [43]).

The overall results obtained in the sub-critical regime with the present intermittency-based hybrid model, in particular at Reynolds numbers 3900 and 20,000, show that a hybrid approach may be suitable to predict such massively separated flows also at moderate Reynolds numbers, as it was observed in [41] with the Detached Eddy Simulation of a circular cylinder flow in the low sub-critical regime.

	$\overline{C}_d$	$\lvert\overline{C_L}\rvert$	C'_l	$-\overline{C}_{pb}$	θ_{sep}	St
Present simulation Re=3900						
$k-\varepsilon$/DVMS	0.967	0.00	0.11	0.85	90	0.20
$k-\varepsilon-\gamma$/DVMS	0.998	0.00	0.11	0.86	88	0.21
Simulation						
LES of Kravchenko [45]	1.04	-	-	0.94	88	0.21
LES of Park [46]	[0.99-1.04]	-	-	[0.89-0.94]	-	0.21
Experiments						
Norberg [42, 43]	0.97	-	0.10	0.84	-	0.21
Ong [47]	-	-	-	-	-	0.21
Present simulation Re=20,000						
$k-\varepsilon$/DVMS	1.102	0.00	0.60	0.85	85	0.22
$k-\varepsilon-\gamma$/DVMS	1.227	0.00	0.48	1.19	89	0.21
Simulation						
LES of Aradag [48]	1.20	-	-	1.25	-	-
VMS-LES of Wornom et al. [49]	1.27	-	0.60	1.09	86	0.19
Experiments						
Norberg [43, 50]	1.16	-	0.46	1.19	-	0.19
Lim [51]	1.19	-	-	1.09	-	-
Present simulations Re=10^5						
$k-\varepsilon$/DVMS	0.660	0.00	0.25	0.60	90	0.21
$k-\varepsilon-\gamma$/DVMS	1.327	0.00	0.77	1.10	90	0.20
Simulation						
LES of Botterill [22]	0.72	-	-	1.82	90	0.25
Experiments						
Norberg [42, 50, 52]	1.21	-	0.52	1.29	-	0.19
Schewe [53]	1.20	-	0.30	-	-	0.20
Roshko [1]	1.20	-	-	1.16	-	-

Table 2: Bulk coefficients of the flow around a circular cylinder at Reynolds numbers 3900, 20,000 and 10^5 (sub-critical regime). $\overline{C}_d$ holds for the mean drag coefficient, $|\overline{C}_l|$ denotes the absolute value of the mean lift coefficient, C'_l is the root mean square of the lift coefficient, $\overline{C}_{p_b}$ is the value of the mean base pressure coefficient, θ_{sep} is the mean separation angle, and St is the vortex shedding frequency. $k-\varepsilon$/DVMS holds for the hybrid model without intermittency modeling, and $k-\varepsilon-\gamma$/DVMS is the present intermittency-based hybrid model.

4.2. Critical regime

The critical Reynolds numbers investigated in this work are 2.5×10^5 and 3.8×10^5, which correspond to those chosen by Lehmkuhl et al. in [18, 19]. In this flow regime, the flow separation is asymmetric, with a partly turbulent boundary layer on one side of the cylinder, and a laminar one on the other side, which is accompanied by a sudden decrease in drag.

The bulk flow parameters are presented in Table 3, together with some experimental data. The LES results of Lehmkuhl et al. [18, 19] obtained on grids of 38.4 million (Re=2.5×10^5) and 48.6 million (Re=3.8×10^5) control volumes, as well as those of Yeon et al. [25] on grids of 67-134 million nodes, are also reported.

Let us first focus on Reynolds number 2.5×10^5. The drag coefficient predicted by the intermittency-based hybrid model is underestimated compared to the experimental data but it is consistent with the LES results of Lehmkuhl et al., and in better agreement with the measurement than that of Yeon et al. It can also be observed that the Strouhal number is in excellent agreement with the experiments, and that the base pressure coefficient is a little underestimated compared to the experimental data and the numerical results of Lehmkuhl et al. but much larger than the value obtained in the LES simulations of Yeon et al. The r.m.s. of the lift coefficient is too large compared to the experimental data and the result of Yeon et al., like the value obtained by Lehmkuhl et al. which is nevertheless less high. It is also important to notice that the hybrid model in its transitional version predicts an asymmetric flow separation with a value of the mean lift coefficient which is no longer very small (see Table 3), although lower than that obtained by Lehmkuhl et al., but more in line with the value of the mean lift coefficient predicted by Yeon at al.

Let us now consider the Reynolds number 3.8×10^5. From Table 3, it can be noticed that the drag coefficient and the base pressure coefficient predicted by the hybrid approach combined with the transitional RANS model are in good agreement with the experimental data and the LES results of Lehmkuhl et al. The mean lift coefficient and the r.m.s. of this coefficient are also in line with those predicted by Lehmkuhl et al. The Strouhal number found corresponds to the first value predicted by Lehmkuhl et al. and is approximately 30 percent lower than the experimental value given in Table 3. It should be mentioned that the power spectrum of the lift fluctuations performed in Lehmkuhl et al. [19] show two distinct peaks contrary to what we can observe in our computations. The scatter observed in the experimental data presented in Fig. 9 in the critical regime shows the difficulty in evaluating this quantity. Again, the intermittency-based hybrid model predicts an asymmetric flow separation with a value of the mean lift coefficient close to that observed by Lehmkuhl et al. (see Table 3).

It is worth mentioning that the hybrid approach, when combined with

the transitional RANS model, significantly improves the prediction of the bulk coefficients for both Reynolds numbers considered. In particular, the baseline RANS model activated in the hybrid approach without transition modeling predicts a turbulent boundary layer on each side of the cylinder with symmetric flow separation, which results in symmetric forces acting on the cylinder surface as indicated by the very small values of the mean lift coefficient given in Table 3.

Name	$\overline{C}_d$	$\lvert\overline{C}_L\rvert$	C'_l	$-\overline{C}_{pb}$	St
Present simulation Re=2.5×10^5					
$k-\varepsilon$/DVMS	0.614	0.00	0.31	0.70	0.30
$k-\varepsilon-\gamma$/DVMS	0.862	0.15	0.65	0.87	0.20
Simulation					
LES of Lehmkuhl et al. [18, 19]	0.83	0.9	0.49	0.99	0.24
LES of Yeon at al. [25]	0.56	0.09	0.12	0.44	0.19
Experiments					
Schewe [53]	1.00	-	0.18	-	0.20
Roshko [1]	1.00	-	-	0.98	-
Present simulations Re=3.8×10^5					
$k-\varepsilon$/DVMS	0.583	0.01	0.34	0.60	0.30
$k-\varepsilon-\gamma$/DVMS	0.458	0.27	0.21	0.53	0.20
Simulation					
LES of Lehmkuhl et al. [18, 19]	0.48	0.25	0.22	0.48	0.24/0.36
Experiments					
Bearman [62]	0.45	-	-	0.51	0.31
Roshko [1]	0.50	-	-	0.55	-

Table 3: Bulk coefficients of the flow around a circular cylinder at Reynolds number 2.5×10^5 and 3.8×10^5 (critical regime). Same symbols as in Table 2

The distribution of the mean pressure coefficient over the upper part and the lower part of the cylinder surface at Reynolds number 2.5×10^5, depicted in Fig. 6, confirms the asymmetric character of the forces acting on the cylinder predicted by the transitional hybrid model, as observed in the experiment, with however a higher value of the minimum of this coefficient compared to the experimental data for both the upper side and the lower side of the cylinder. On the contrary, the hybrid model without transition modeling predicts a symmetric mean pressure coefficient with a larger deviation at the rear of the cylinder compared to the measurements.

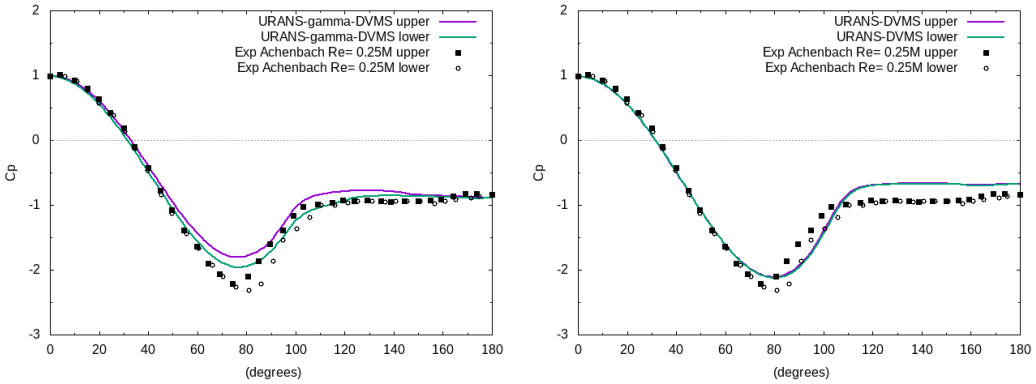

Figure 6: Flow past a cylinder at Reynolds number 2.5×10^5 (critical regime): distribution over the upper part (purple) and the lower part (green) of the cylinder surface of the mean pressure coefficient obtained with the present intermittency-based hybrid model (left) and its counterpart without transition (right), compared to experimental data (Achenbach [56]).

4.3. Super-critical regime

Two super-critical Reynolds numbers are considered in this work, namely 7.2×10^5 and 10^6. In the super-critical regime, a laminar-turbulent transition occurs on each side of the cylinder, resulting in late flow separation and a thin wake, as well as symmetric forces acting on the cylinder surface.
The main bulk coefficients obtained in our simulations are shown in Table 4. They are compared with experimental data and the LES results of Lehmkuhl et al. [18, 19] on a grid of 89.4×10^6 control volumes, the LES results of Kim et al. [54] on a mesh of 6.8×10^6 cells, and those of Catalano et al. on a grid of 2.3×10^6 points.

Let us first analyze the results obtained at Reynolds number 7.2×10^5 by the hybrid model in its transitional version. The drag coefficient is in fairly good agreement with the experiments and the LES results of Lehmkuhl et al., with a slighlty higher value of the predicted drag, except for the data from Roshko. As observed in experimental studies [30, 56, 59, 61], this value is much smaller than those obtained in the critical regime presented in Table 3. As for the Strouhal number, its value is a little too low compared to the experimental data but consistent with that predicted by Lehmkuhl et al.. The r.m.s. of the lift coefficient is reasonably small, and more in line with the experimental measurement than the LES results of Lehmkuhl et al. The

base pressure coefficient matches that of Lehmkuhl et al. and is in good agreement with the experimental data.

Let us now consider the results predicted by the intermittency-based hybrid model at Reynolds number 10^6 presented in Table 4. It can be first noticed that the value of the drag coefficient is higher that the experimental results of Shih [29], Schewe [30] and Gölling [31], but is close to those of Roshko [1] and falls within the scatter of the experimental data compiled by Zdravkovich [2], and is also in line with the LES results of Kim et al. and those of Catalano et al. The r.m.s. of the lift coefficient, very small, is more consistent with the experimental result of Schewe than the measurements reported by Zdravkovich. The base pressure coefficient is within the range of experimental data given by Zdravkovich, although somewhat lower than the measurements of Shih and Roshko, and that predicted in the LES simulations reported in Table 4. The separation angle is in good agreement with the experiments. The Strouhal number obtained corresponds to the highest experimental values presented in Table 4. It can be noticed that two values of the Strouhal number are reported in some of the presented experiments which correpond to the sudden decrease of the vortex shedding frequency in the super- to trans-critical transitional range. This is not observed in our numerical results and in those of Catalano et al., as well as in the experiment of Schewe for which this sharp drop of the Strouhal number is measured at higher Reynolds numbers. However, according to the results of our simulations in the super-critical regime, one can note a strong increase in the Strouhal number compared to the critical cases considered in our study (see Table 3), as it was observed in experiments [30, 62] which report an increase in the vortex shedding frequency when the drag coefficient is approaching its minimum value.

It can also be noted that the mean lift coefficient predicted by the present intermittency-based hybrid model is very small for both Reynolds numbers, which confirms the symmetric flow separation as can be seen in Fig. 10.

Due to the inability of the baseline $k-\epsilon$ model to properly account for the laminar-turbulent transition in the boundary layer that characterizes this flow regime, the hybrid model without transition modeling provides, for both considered Reynolds numbers, poor results which are drastically improved by the transitional hybrid model.

The good overall prediction of the bulk coefficients obtained by the hybrid model based on intermittency is confirmed in Fig. 7 which shows the distribution over the cylinder surface of the mean pressure coefficient at Reynolds

	$\overline{C}_d$	$\lvert\overline{C_L}\rvert$	C'_l	$-\overline{C}_{pb}$	θ_{sep}	St
Present simulation Re=7.2×10^5						
$k-\varepsilon$/DVMS	0.548	0.01	0.31	0.50	110	0.32
$k-\varepsilon-\gamma$/DVMS	0.246	0.00	0.01	0.22	125	0.43
Simulation						
LES of Lehmkuhl et al. [18, 19]	0.21	0.02	0.07	0.22	-	0.45
Experiments						
Schewe [30]	0.22	-	0.02	-	-	0.47
Gölling [31]	0.21	-	-	-	-	0.49
Roshko [1]	0.27	-	-	0.24	-	-
Present simulation Re=10^6						
$k-\varepsilon$/DVMS	0.536	0.03	0.30	0.51	110	0.34
$k-\varepsilon-\gamma$/DVMS	0.289	0.03	0.04	0.25	128	0.50
Simulation						
LES of Kim and Mohan [54]	0.27	-	0.12	0.28	108	-
LES of Catalano et al. [55]	0.31	-	-	0.32	-	0.35
Experiments						
Shih [29]	0.24	-	-	0.33	-	-
Schewe [30]	0.22	-	0.02	-	-	0.44
Gölling [31]	0.22	-	-	-	130	0.12/0.47
Zdravkovich [2]	0.2-0.4	-	0.1-0.15	0.2-0.34	-	0.18/0.50
Roshko [1]	0.29	-	-	0.34	-	-

Table 4: Bulk coefficients of the flow around a circular cylinder at Reynolds numbers 7.2×10^5 and 10^6 (super-critical regime). Same symbols as in Table 2

number 10^6. The results obtained by the hybrid model without transition are also reported, again showing the improvement brought by the intermittency-based hybrid model.

4.4. Drag crisis, increase in Strouhal number, wake and shear layer instabilities

We now evaluate the prediction of some important phenomena characterizing the flow around a circular cylinder provided by the hybrid model with and without transition modeling.

The drag crisis phenomenon, which is characterized by a sudden drop in the mean drag coefficient at critical Reynolds numbers as observed in various experimental studies (see, for example, [30, 56, 59, 61]), is a difficult mechanism to predict in numerical simulations. Few works based on three-dimensional calculations have dealt with this phenomenon [18, 19, 20, 21, 22, 23, 24], and for the majority of them the results turned out to be rather inac-

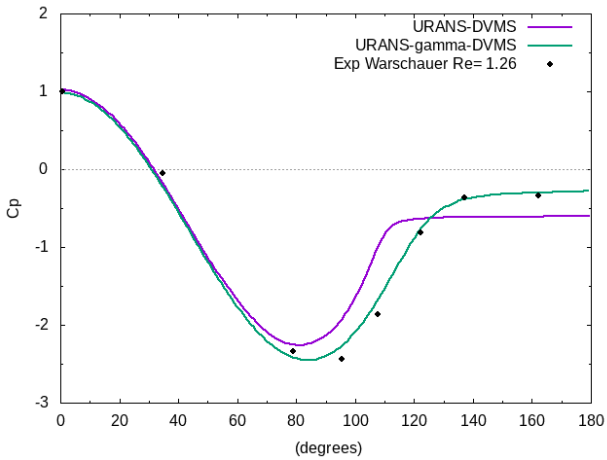

Figure 7: Flow past a cylinder at Reynolds number 10^6 (super-critical regime): distribution over the cylinder surface of the mean pressure coefficient obtained with the hybrid model with and without transition modeling (in green and purple, respectively), compared to experimental data (Warschauer [57]).

curate. A successful work on the subject is that of Lehmkuhl et al. [18, 19] in which, with LES calculations on fine meshes up to nearly 90 million control volumes, a prediction of the drag crisis in good agreement with the experimental results was obtained.
In Fig. 8, the prediction of the drag crisis by the proposed intermittency-based hybrid model and its counterpart without intermittency modeling is presented, as well as the numerical results of Lehmkuhl et al. [18, 19]. Various experimental data are also reported. It turns out that the results obtained with the intermittency-based hybrid model are in good accordance with the experimental measurements, with a correct capture of the drag crisis phenomenon, comparable to that obtained by Lehmkuhl et al. It can also be noticed that the use of intermittency modeling in our hybrid simulations drastically improves the prediction accuracy. These results are all the more satisfactory as the meshes used are not very fine (approximately 0.6 million nodes). This confirms the usefulness of hybrid turbulence approaches to simulate turbulent wall flows at a lower cost.

Another important physical phenomenon occurring in the critical regime is a sharp increase in the Strouhal number as observed in several experimental studies (see, for example, [30, 31, 43, 56, 62]). Among the very few works

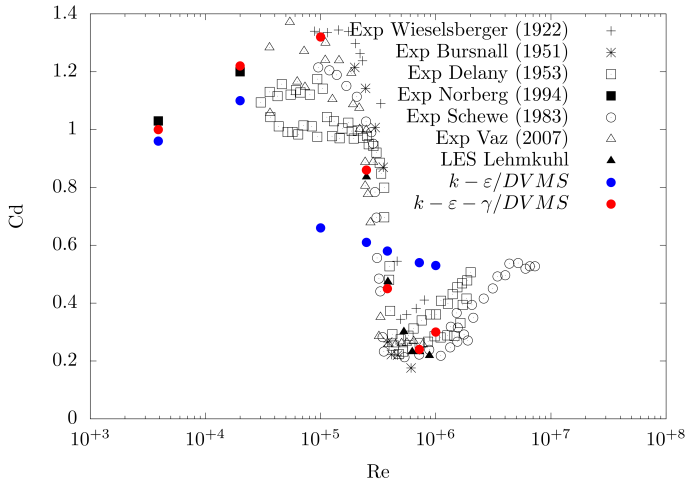

Figure 8: Impact of the intermittency model (in red) on the drag crisis prediction, in contrast with the same hybrid model without intermittency modeling (in blue). Comparison with experimental data (Wieselsberger [58], Bursnall [59], Delany [60], Norberg [43], Schewe [30], Vaz [61]) and the LES results of Lehmkuhl et al. [18, 19].

based on three-dimensional simulations having dealt with this phenomenon [18, 19, 20, 24, 25], we can still mention the numerical studies by Lehmkuhl et al. [18, 19], based on LES computations on fine grids, which are certainly the most accomplished.
The Strouhal number obtained with the proposed intermittency-based hybrid model and its counterpart without intermittency modeling is summarized in Fig. 9. The LES results of Lehmkuhl et al. [19] are also reported, along with various experimental measurements. The dispersion observed in the experimental data is mainly due to the critical nature of the flow, which makes the repeatability of the results more difficult. Nevertheless, it can be observed that the hybrid approach based on transition modeling predicts reasonably well the rise of the Strouhal number with a correct amplitude, unlike the same hybrid approach without intermittency modeling, although the Strouhal number at Reynolds 3.8×10^5 is probably lower than expected.

The instantaneous vorticity magnitude field with an extended region downstream in the wake obtained with the hybrid approach based on intermittency modeling is also shown in Fig. 10 for the various Reynolds numbers

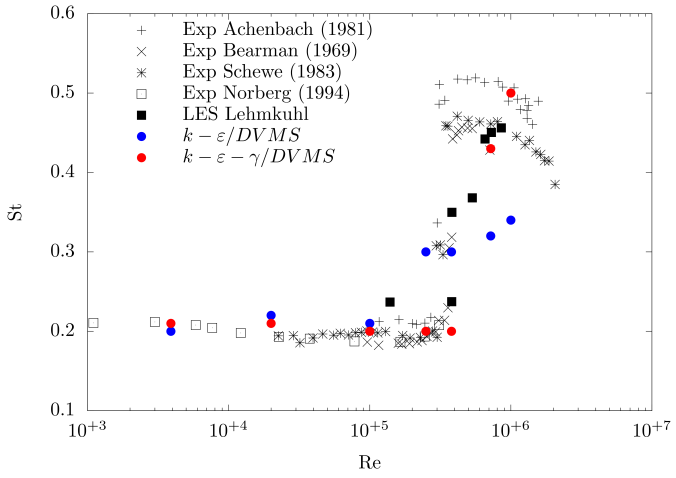

Figure 9: Impact of the intermittency model (in red) on the prediction of the vortex shedding frequency, in contrast with the same hybrid model without intermittency modeling (in blue). Comparison with experimental data (Achenbach [56], Bearman [62], Schewe [30], Norberg [52]) and the LES results of Lehmkuhl et al. [19].

considered in this work. In addition, sequences of instantaneous vorticity fields are given in Figs. 11, 12 and 13 for Reynolds numbers 10^5 (sub-critical regime), 2.5×10^5 (critical regime) and 10^6 (super-critical regime) regarding the Kelvin-Helmholtz frequency f_{KH} (determined later in this section) for the first Reynolds number mentioned above and the vortex shedding frequency f_{vs} for the other two Reynolds numbers. Some well known flow characteristics can be observed, such as a variation, according to the Reynolds number, in the location at which the boundary layer separates, with an early separation in the sub-critical regime and a late separation in the super-critical regime. One can also notice the Von Karman vortex street behind the cylinder at all Reynolds numbers with clockwise rotating vortices (at the top of the wake) and counterclockwise rotating vortices (at the bottom of the wake), as well as a reduction in the wake width with the Reynolds number. The streamwise distance between the emitted vortices also diminishes which is related to the increase in the Strouhal number, due to the reduction of the coherent structures. The wake then has a more compact appearance with more vortices for the same length with respect to lower Reynolds numbers. These physical features, as well as the three-dimensional character of the flow and the wake vortical structures, can be highlighted with the visualization

of the Q-criterion contours for each flow regime (sub-critical, critical and super-critical), see Fig. 14.

It should also be mentioned that the proposed intermittency-based hybrid model was able to capture shear layer instabilities, which is clearly visible at the Reynolds number 10^5, as can be seen in Figs. 10, 11 and 14. These Kelvin-Helmholtz instabilities, which play an important role in the transition to turbulence, lead to the formation of small vortices which are convected downstream and feed the larger Von Karman vortices. In order to compute the Kelvin-Helmholtz instabilities frequency, one way consists in computing the energy spectrum at a sensor located in the shear layers or close to them, in our case the point $(0.3, 0.5, 0)$ was chosen (point S in the top left image of Fig. 11), where the cylinder axis corresponds to $x = 0$ and $y = 0$, and the cylinder diameter is 1. The resulting spectral analysis is shown in Fig. 15, from which a ratio of the Kelvin-Helmholtz frequency to that of the vortex shedding (f_{KH}/f_{vs}) equal to 37.5 has been deduced. This value is between that deduced from the scaling proposed by Kourta et al. [63], $f_{KH}/f_{vs} = 0.095Re^{0.5}$, which in our case would give a ratio equal to 30.1, and the one deduced from the scaling proposed by Prasad and Williamson [64], $f_{KH}/f_{vs} = 0.0235Re^{0.67}$, leading to a ratio equal to 52.6.

We would like to mention that the objective of the simulations carried out in this work is to capture the main physical features of the flow using not too computationaly expensive three-dimensional grids, together with a hybrid model, which allow the prediction of important phenomena and main flow outputs of interest to engineers. The present results show that important bulk coefficients, flow characteristics, and physical phenomena like drag crisis are reasonably predicted, with however less flow details captured in the present simulations compared to LES computations carried out on finer grids, such as in [18, 19] for example.

5. Concluding remarks

A hybrid method blending a transitional RANS model and a DVMS approach has been proposed and investigated in the simulation of the flow around a circular cylinder using a mixed finite element-finite volume framework. The RANS model is equipped with an intermittency equation so that the hybrid approach can handle laminar to turbulent transition. An other positive feature is that the DVMS approach is integrated in the hybridization strategy for the closure of the LES part. In order not to degrade the

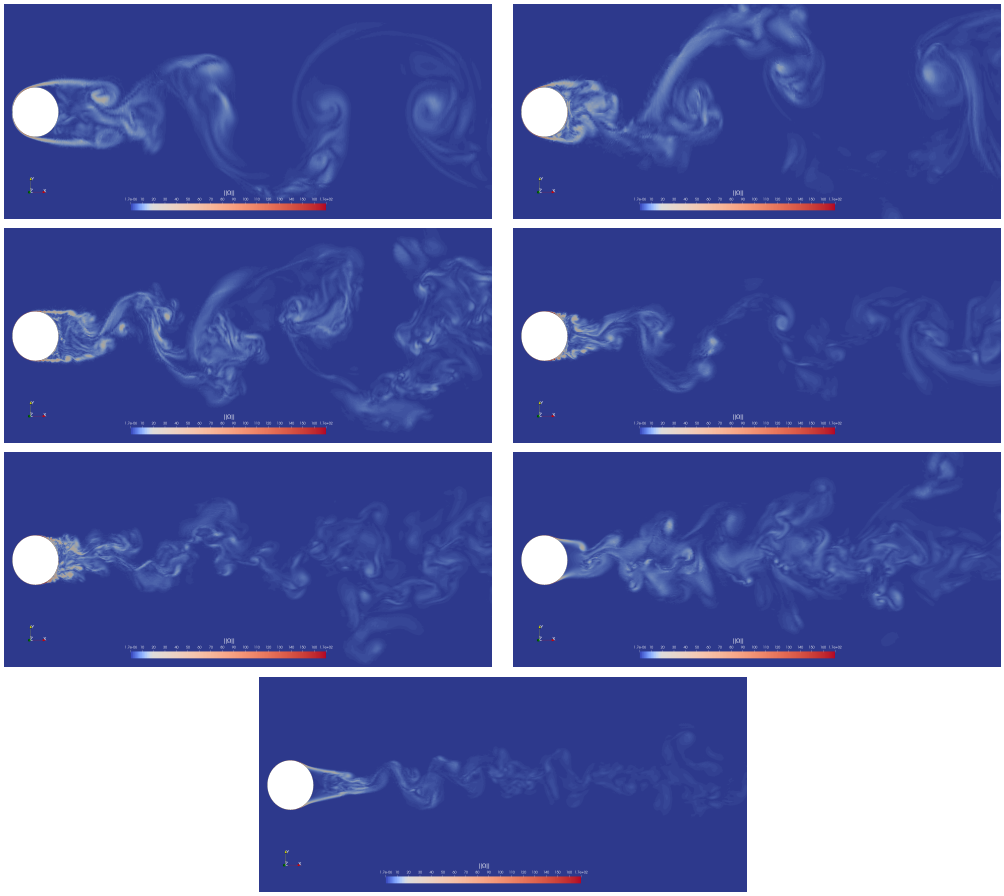

Figure 10: Instantaneous vorticity magnitude in spanwise-cross section for various Reynolds numbers from sub-critical to super-critical flow regimes (from left to right, top then bottom: Re=3900, Re=20,000, Re=10^5, Re=2.5×10^5, Re=3.8×10^5, Re=7.2×10^5, Re=10^6).

performance of the turbulence model used, the numerical model is based on a second-order accurate numerical scheme stabilized by a tunable numerical diffusion proportional to high-order space derivatives.

This hybrid model has been applied to the simulation of the flow past a circular cylinder for flow regimes ranging from sub-critical to super-critical. The main flow characteristics are captured and the prediction of the bulk coefficients in all the considered flow regimes is in overall good agreement with the measurements and the results of other numerical simulations in the literature. The challenging problem of the drag crisis phenomenon is in

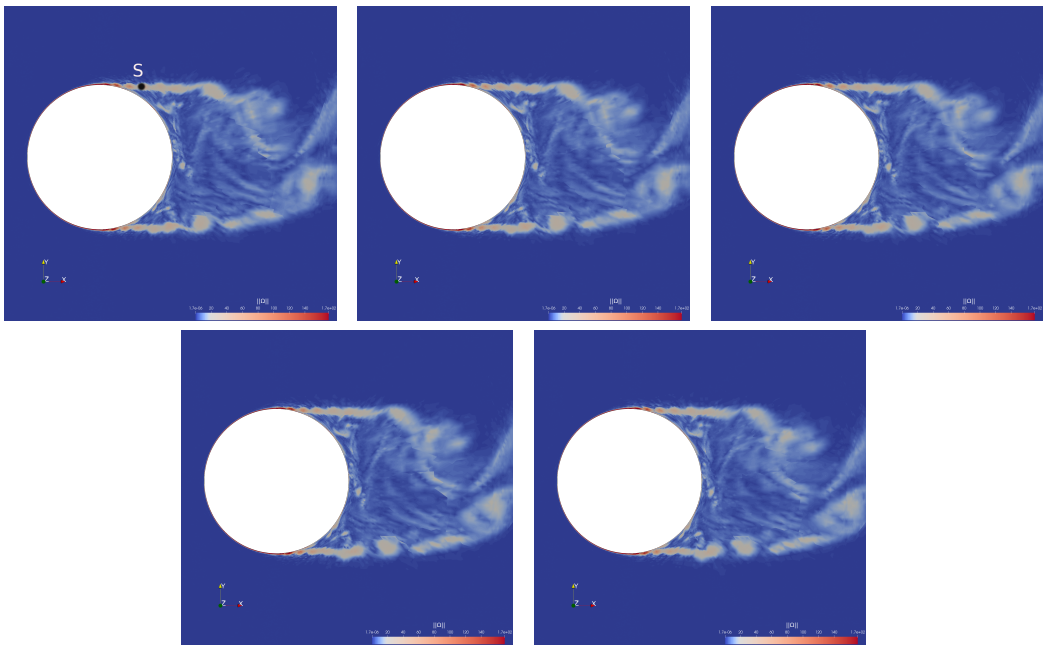

Figure 11: Sequence of instantaneous vorticity magnitude fields in spanwise-cross section for Reynolds number 10^5 with time sampling equal to $(4f_{KH})^{-1}$. The point S in the top left image denotes the sensor location to compute the energy spectrum for the purpose of evaluating the Kelvin-Helmholtz frequency.

particular correctly reproduced, as well as the sharp increase in the vortex shedding frequency when the drag coefficient reaches its minimum. It has also been observed that the main bulk flow quantities can be reasonably predicted even with the use of relatively coarse meshes. This confirms the fact that, at high Reynolds numbers, the hybrid approach is suitable if one wants to avoid the use of very refined grids leading to huge computational requirements and costs. On the other hand, the wide range of flow regimes investigated in this work shows that a hybrid approach can also be suitable for predicting flows past an obstacle at moderate Reynolds numbers. It also turned out that the use, in the hybrid method, of a RANS model able to take into account the laminar to turbulent transition is essential to successfully simulate massively separated flows such those considered in this work. These results are encouraging in the perspective of applying this hybrid strategy to the simulation of complex engineering problems, such as flows over three-dimensional airfoils in incidence or flows in rotating machines (helicopters,

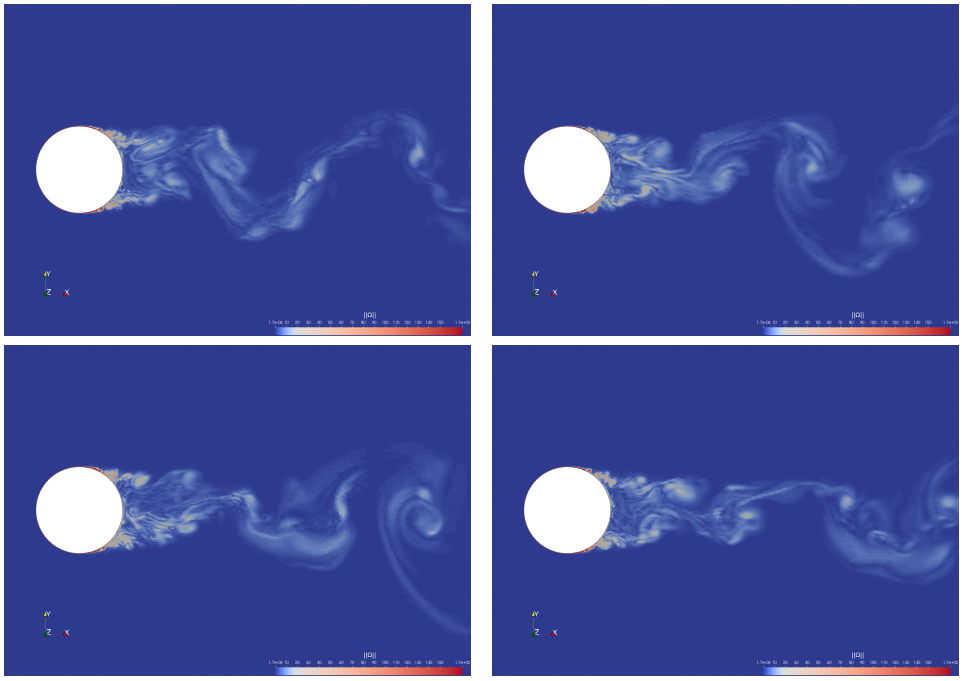

Figure 12: Sequence of instantaneous vorticity magnitude fields in spanwise-cross section for Reynolds number 2.5×10^5 with time sampling equal to $(3f_{vs})^{-1}$.

drones).

Acknowledgements

This work was supported by the ANR NORMA project, grant ANR-19-CE40-0020-01 of the French National Research Agency. The authors gratefully acknowledge GENCI for granted access to HPC resources through IDRIS (grant 2022-A0132A05067) and CINES (grants 2021-A0102A06386 and 2020-A0092A05067).

References

[1] Roshko, A., 1961, Experiments on the flow past a circular cylinder at very high Reynolds number, J. Fluid Mech. 10, 345-356.

[2] Zdravkovich, M. M., 1997, Flow around circular cylinder: Volume 1: Fundamentals, Oxford University Press.

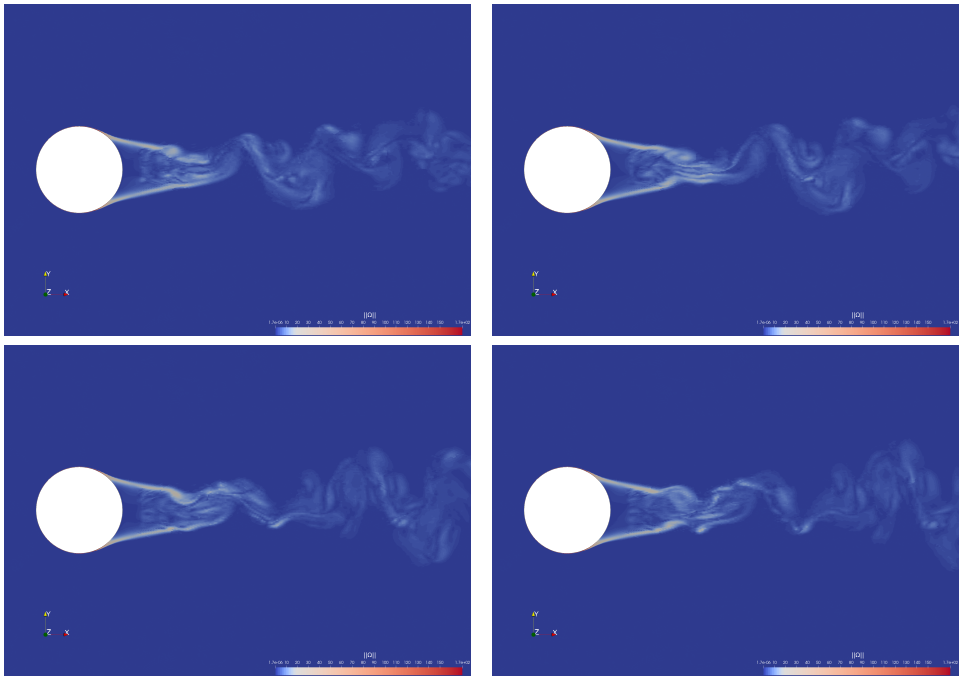

Figure 13: Sequence of instantaneous vorticity magnitude fields in spanwise-cross section for Reynolds number 10^6 with time sampling equal to $(3f_{vs})^{-1}$.

[3] Achenbach, E., 1975, Total and local heat transfer from a smooth circular cylinder in cross-flow at high Reynolds number, International Journal of Heat and Mass Transfer 18, 1387-1396.

[4] Sagaut, P., Deck, S., Terracol, M., 2006, Multiscale and Multiresolution Approaches in Turbulence, Imperial College Press,London.

[5] Froehlich, J., von Terzi, D., 2008, HybridLES/RANS methods for the simulation of turbulent flows, Progress in Aerospace Sciences 44(5), 349-377.

[6] Chaouat, B., 2017 The State of the Art of Hybrid RANS/LES Modeling for the Simulation of Turbulent Flows, Flow Turbulence Combust 99, 279-327.

[7] Menter, F., Hüppe, A., Matyushenko, A., Kolmogorov, D., 2021, An Overview of Hybrid RANS-LES Models Developed for Industrial CFD, Appl. Sci. 11, 2459.

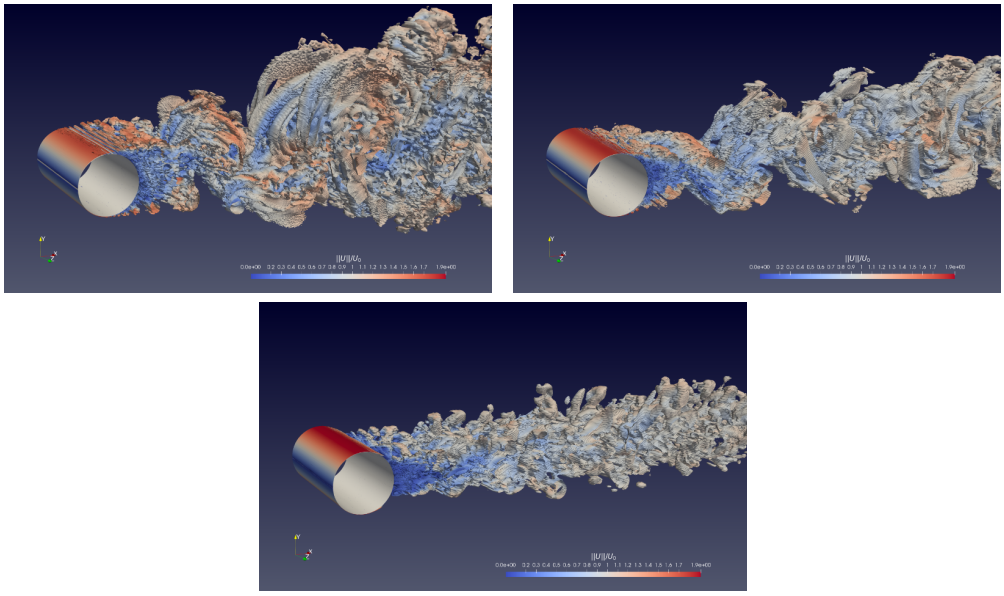

Figure 14: Q-criterion contours ($Q = 0.5$) colored with the norm of the velocity for Reynolds numbers 10^5, 2.5×10^5 and 10^6(respectively from left to right, top then bottom) corresponding to the sub-critical, critical and super-critical regimes.

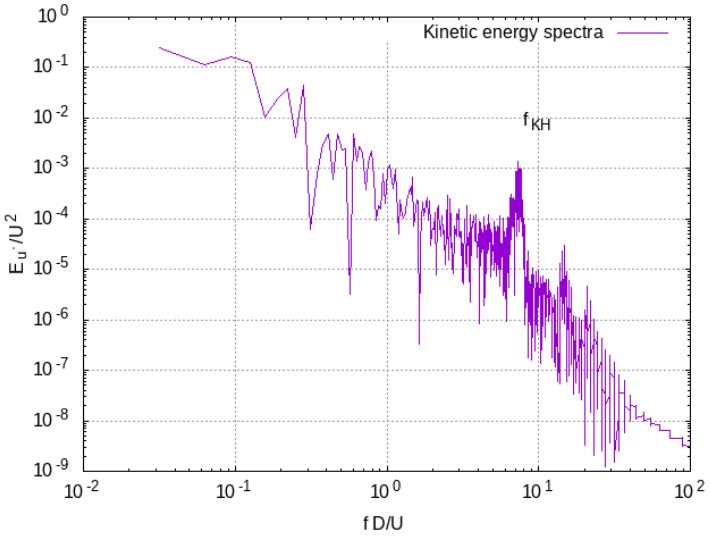

Figure 15: Shear layer instabilites frequency at Reynolds number 10^5. The Kelvin-Helmholtz frequency is noted f_{KH} in the spectrum.

[8] Moussaed, C., Wornom, S., Salvetti, M.V., Koobus, B. and Dervieux, A., 2014, Impact of dynamic subgrid-scale modeling in variational multiscale large-eddy simulation of bluff body flows, Acta Mechanica 225, 3309-3323.

[9] Moussaed, C., Salvetti, M.V., Wornom S., Koobus, B. and Dervieux, A., 2014, Simulation of the flow past a circular cylinder in the supercritical regime by blending RANS and variational-multiscale LES models, Journal of Fluids and Structures 47, 114-123.

[10] Goldberg, U., Peroomian, O. and Chakravarthy, S., 1998, A wall-distance-free $k-\varepsilon$ model with Enhanced Near-Wall Treatment, Journal of Fluids Engineering 120, 457–462.

[11] Koobus, B.,Farhat, C., 2004, A variational multiscale method for the large eddy simulation of compressible turbulent flows on unstructured meshes application to vortex shedding, Computer Methods in Applied Mechanics and Engineering 193, 1367-1383.

[12] Germano, M., Piomelli, U.,Moin, P., Cabot,W.H., 1991, A dynamic subgrid-scale eddy viscosity model, Phys. Fluids A 3, 1760-1765.

[13] Lilly, D. K., 1992, A proposed modification of the Germano subgrid-scale closure method, Phys. Fluids A4(3), 633–635.

[14] Akhter, M.N., Funazaki, K.I., 2007, Development of Prediction Method of Boundary Layer Bypass Transition using Intermittency Transport Equation, International Journal of Gas Turbine, Propulsion and Power Systems 1, 30–37.

[15] Akhter, M.N., Yamada, K., Funazaki, K.I., 2009, Numerical Simulation of Bypass Transition by the Approach of Intermittency Transport Equation, Journal of Fluid Science and Technology 4, 524-535.

[16] Akhter, M.N., Ali, M., Funazaki, K.I., 2015, Numerical simulation of heat transfer coefficient on turbine blade using intermittency factor equation. Procedia Engineering 105, 495-503, The 6th BSME International Conference on Thermal Engineering.

[17] Menter, F.R., Smirnov, P.E., Liu, T., Avancha, R., 2015, A One-Equation Local Correlation-Based Transition Model. Flow Turbulence Combust 95, 583619.

[18] Lehmkuhl, O., Rodriguez, I., Borrell, R., Chiva, J., Oliva, A., 2014, Unsteady forces on a circular cylinder at critical Reynolds numbers, Physics of Fluids 26, 125110.

[19] Rodriguez, I., Lehmkuhl, O., Chiva, J., Borrell, R., Oliva, A., 2015, Physics of Fluids 26, 125110. On the flow past a circular cylinder from critical to super-critical Reynolds numbers: Wake topology and vortex shedding, International Journal of Heat and Fluid Flow 55, 91–103.

[20] Wen, P., Qiu, W., 2017, Investigation of drag crisis phenomenon using CFD methods, Applied Ocean Research 67, 306-321.

[21] A S Stabnikov and A V Garbaruk, 2020, J. Phys.: Conf. Ser. 1697 012224.

[22] Botterill, N., Owen, J.S., Morvan, H.P., 2009, Investigation Into Numerical Modeling Of The Drag Crisis For Circular Cylinders, 5th European & African conference on wind engineering : Florence Italy, July 19th-23rd 2009, conference proceedings.

[23] Bharara, S., 2016, Simulation of Drag Crisis in flow past a circular cylinder using 3-D computations, International Journal of Aerospace and Mechanical Engineering 3, 17–19.

[24] Lloyd, T.P., James, M., 2015, Large eddy simulations of a circular cylinder at Reynolds numbers surrounding the drag crisis, Applied Ocean Research 59, 676–686.

[25] Yeon, S.M., Yang, J., Stern, F., 2016, Large–eddy simulation of the flow past a circular cylinder at sub– to super–critical Reynolds numbers, Applied Ocean Research 59, 663-675.

[26] Dick, E., Kubacki, S., 2017, Transition Models for Turbomachinery Boundary Layer Flows: A Review, Int. J. Turbomach. Propuls. Power, 2, 4.

[27] Di Pasquale, D., Rona, A., Garrett, S.J., 2009, A selective review of CFD transition models, 39th AIAA Fluid Dynamics Conference, AIAA paper number 2009-3812.

[28] Abu-Ghannam, B.J., Shaw, R., 1980, Natural Transition of Boundary Layers-The Effects of Turbulence, Pressure Gradient, and Flow History, Journal of Mechanical Engineering Science 22(5), 213–228.

[29] Shih, W.C.L., Wang, C., Coles, D., Roshko, A., 1993, Experiments on flow past rough circular cylinders at large Reynolds numbers, Journal of Wind Engineering and Industrial Aerodynamics 49(1), 351–368.

[30] Schewe, G., 1983, On the force fluctuations acting on a circular cylinder in crossflow from subcritical up to transcritical Reynolds number, Journal of Fluid Mechanics 133, 265–285.

[31] Gölling, B., 2006, Experimental investigations of separating boundary-layer flow from circular cylinder at Reynolds numbers from 10^5 up to 10^7, Proceedings of IUTAM Symposium on One Hundred Years of Boundary Layer Research, 455–462.

[32] Hughes, T. J. R., Mazzei, L., and Jansen, K. E., 2000, Large eddy simulation and the variational multiscale method, Comput Vis Sci 3, 47-59.

[33] Smagorinsky, J., 1963, General circulation experiments with the primitive equations, Monthly Weather Review 91(3), 99-164.

[34] Nicoud, F., and Ducros, F., 1999, Subgridscale stress modelling based on the square of the velocity gradient tensor, Flow, Turbulence and Combustion 62, 183-200.

[35] Camarri, S., Salvetti, M.V., Koobus, B., Dervieux, A., 2004, A low diffusion MUSCL scheme for LES on unstructured grids, Comput. Fluids 33, 1101-1129.

[36] Roe, P.L., 1981, Approximate Riemann solvers, parameters, vectors and difference schemes, J. Comput. Phys. 43, 357-371.

[37] Schall, E., Viozat, C., Koobus, B., Dervieux, A., 2003, Computation of low Mach thermical flows with implicit upwind methods, International Journal of Heat and Mass Transfer 46, 3909-3926.

[38] Van Leer, B., 1977, Towards the ultimate conservative scheme. IV: a new approach to numerical convection, J. Comput. Phys. 23, 276-299.

[39] Martin, R., Guillard, H., 1996, A second-order defect correction scheme for unsteady problems, Comput. Fluids 25(1), 9-27.

[40] Ouvrard, H., Koobus, B., Dervieux, A., Salvetti, M.V., 2010, Classical and variational multiscale LES of the flow around a circular cylinder on unstructured grids, Computers & Fluids 39(7), 1083–1094.

[41] D'Alessandro, V., Montelpare, S., Ricci, R., 2016, Detached-Eddy Simulations of the flow over a cylinder at Re=3900 using OpenFOAM, Computers and Fluids 136, 152–169.

[42] Norberg, C., 1987, Effect of Reynolds number and a low-intensity freestream turbulence on the flow around a circular cylinder, (Publikation; Vol. 87, No. 2), Chalmers University of Technology.

[43] Norberg, C., 1993, Pressure Forces on a Circular Cylinder in Cross Flow, In: Eckelmann, H., Graham, J.M.R., Huerre, P., Monkewitz, P.A. (eds) Bluff-Body Wakes, Dynamics and Instabilities, International Union of Theoretical and Applied Mechanics, Springer, Berlin, Heidelberg.

[44] Behara, S., Mittal, S., 2011, Transition of the boundary layer on a circular cylinder in the presence of a trip, Journal of Fluids and Structures 27(5–6), 702–715.

[45] Kravchenko, A., Moin, P., 2000, Numerical studies of flow over a circular cylinder at $\mathrm{Re}_D = 3900$, Physics of Fluids 12, 403–417.

[46] Park, N., Lee, S., Lee, J., Choi, H., 2006, A dynamic subgrid-scale eddy-viscosity model with a global model coefficient, Physics of Fluids 18, 125109.

[47] Ong, L., Wallace, J., 1996, The velocity field of the turbulent very near wake of a circular cylinder, Experiments in Fluids 20, 441-453.

[48] Aradag, S., 2009, Unsteady turbulent vortex structure downstream of a three dimensional cylinder, J. Therm. Sci. Technol. 29(1), 91-98.

[49] Wornom, S., Ouvrard, H., Salvetti, M.V., Koobus, B., Dervieux, A., 2011, Variational multiscale large-eddy simulations of the flow past a circular cylinder: Reynolds number effects, Computers & Fluids 47(1), 44–50.

[50] Norberg, C., 2003, Fluctuating lift on a circular cylinder : review and new measurements, Journal of Fluids and Structures 17(1), 57-96.

[51] Lim, H., Lee, S., 2002, Flow Control of Circular Cylinders with Longitudinal Grooved Surfaces, AIAA J. 40, 2027–2036.

[52] Norberg, C., 1994, An experimental investigation of the flow around a circular cylinder: Influence of aspect ratio, Journal of Fluid Mechanics 258, 287–316.

[53] Schewe, G., 1995, On the force fluctuations acting on a circular cylinder in crossflow from subcritical up to transcritical Reynolds numbers, Journal of Fluid Mechanics 133, 265-285.

[54] Kim, S.E., Mohan, L.S., 2005, Prediction of Unsteady Loading on a Circular Cylinder in High Reynolds Number Flows Using Large Eddy Simulation, Proceedings of the International Conference on Offshore Mechanics and Arctic Engineering - OMAE 3.

[55] Catalano, P., Wang, M., Iaccarino, G., Moin, P., 2003, Numerical simulation of the flow around a circular cylinder at high Reynolds numbers, International Journal of Heat and Fluid Flow 24, 463-469.

[56] Achenbach, E., Heinecke, E., 1981, On vortex shedding from smooth and rough cylinders in the range of Reynolds numbers 6×10^3 to 5×10^6, Journal of Fluid Mechanics 109, 239–251.

[57] Warschauer, K.A., Leene, J.A., 1971, Experiments on mean and fluctuating pressures of circular cylinders at cross flow at very high Reynolds numbers, In: Proceeding International Conference on Wind Effects on Buildings and Structures, Saikon, Tokyo, pp.305-315 (see also Zdravkovich,1997).

[58] Wieselsberger, C., 1922, New data on the laws of fluid resistance, Tech. Rep. TN-84, NACA.

[59] Bursnall, W., Loftin, L. J., 1951, Experimental investigation of the pressure distribution about a yawed circular cylinder in the critical Reynolds number range, Tech. Rep. NACA N2463, NACA.

[60] Delany, N., Sorensen, N., 1953, Low-speed drag of cylinders of various shapes, Tech. Rep. NACA TN3038, NACA.

[61] Vaz, G., Mabilat, C., van der Wal, R., Gallagher, P., 2007, Viscous flow computations on smooth cylinders: A detailed numerical study with validation, In: 26th International Conference on Offshore Mechanics and Artic Engineering, OMAE2007, San Diego, California.

[62] Bearman, P. W., 1969, On vortex shedding from a circular cylinder in the critical Reynolds number regime, J. Fluid Mech 37, 577-585.

[63] Kourta, A., Boisson H.C., Chassaing P., Ha Minh H., 1987 Nonlinear interaction and the transition to turbulence in the wake of a circular cylinder, J. Fluid Mech 181, 141–161.

[64] Prasad, A., Williamson, C.H.K., 1997, The instability of the shear layer separating from a bluff body flow, J. Fluid Mech 333, 375–402.

[65] Travin, A., Shur, M., Strelets, M., Spalart, P., 2000, Detached-Eddy Simulations Past a Circular Cylinder, Flow, Turbulence and Combustion 63: 293-313, 1999.

[66] El Akoury, R., Braza, M., Mockett, C., Perrin, R., Reimann, T., Revell, A., Craft, T., Laurence, D., Hoarau, Y., Thiele, F., 2009, IV Applications - Test Cases, 1 Circular cylinder Flow, Notes on Numerical Fluid Mechanics and Multidisciplinary Design, Vol. 103, Publisher Springer, ISBN 978-3-540-92772-3.